Dedicated to innovation in aerospace

NLR-TP-2022-004 | February 2022

Development of a Liquid Hydrogen-Based Fuel Cell System for the HYDRA-2 Drone

CUSTOMER: NLR

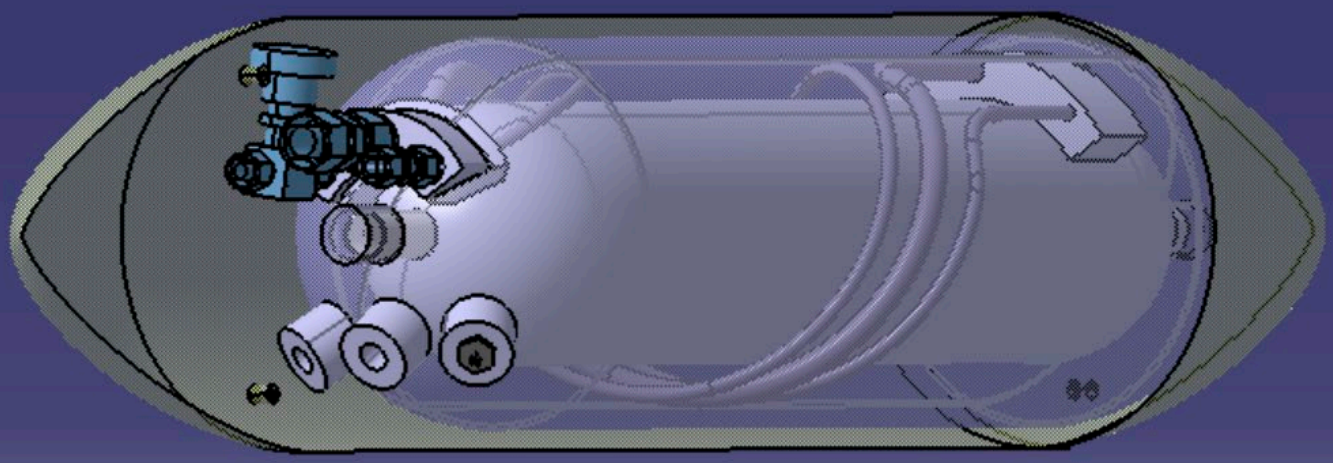

Royal NLR - Netherlands Aerospace Centre

Dedicated to innovation in aerospace

Development of a Liquid Hydrogen-Based Fuel Cell System for the HYDRA-2 Drone

Hydra-2, NLR's hydrogen propelled flight platform. The bottom fairing contains the storage compartment holding the hydrogen tank

Problem area

The aviation sector is actively pursuing a reduction to its environmental footprint. Liquid hydrogen based propulsion is one of the key innovative technologies that is currently being explored. Before this technology can be introduced into the aviation sector several obstacles have to be overcome such as infrastructure, propulsion system, and architecture of aircraft. To gain experience with the technology NLR is currently deploying a ground-based infrastructure and developing a flight platform HYDRA-2B, see figure. The HYDRA-2B platform is a parallel development focused on cryogenic hydrogen next to HYDRA-2A that runs on compressed hydrogen. For HYDRA-2B a cryogenic fuel storage is necessary with a minimum capacity for a flight time of two hours.

REPORT NUMBER
NLR-TP-2022-004

AUTHOR(S)
P.C. de Boer
A.J. de Wit
R.C. van Benthem

REPORT CLASSIFICATION
UNCLASSIFIED

DATE
February 2022

KNOWLEDGE AREA(S)
Computational Mechanics and Simulation Technology
Aerospace Collaborative Engineering and Design

DESCRIPTOR(S)
LH2
fuel tank
HYDRA-2
liquid hydrogen propulsion drone

Description of work

A 4 liter liquid hydrogen storage tank that fits inside the fearing of HYDRA-2 has been designed together with a light weight conditioning system. A trade-off study between single and double wall LH2 tanks has been conducted where different geometries were compared against boil-down time of the hydrogen (the time it takes for all hydrogen to boil-off). The material trade-off for the tank structure was driven by weight, manufacturing and thermal considerations as well as the material's resistance to hydrogen embrittlement. Furthermore, relevant design and certification requirements were determined for the design of the tank and conditioning system. Finally, a preliminary outline of an Liquid Hydrogen propulsion system is described and remaining challenges and improvements are collected and outlined.

Results and conclusions

A flight time of two hours with HYDRA-2 using LH2 for propulsion is only feasible with a double wall tank structure and a light weight conditioning system considering the design requirements of the HYRDRA-2. Aluminium 5083-0 is chosen as the main building material because of favourable mechanical properties at cryogenic temperatures and it's resistance against hydrogen embrittlement. The main driver for tank structural sizing is weldability of the tank wall. Hence, for this particular design structural requirements based on pressure, thermal and dynamic loading did not drive the design of the tank and conditioning system.

Applicability

The work carried out in this research can be used for the construction of a liquid hydrogen storage tank and light weight conditioning system to enable flight testing with liquid hydrogen at NLR's facilities. The developed design philosophy can be used to assist in the design of larger liquid hydrogen tank structures that would for example use advanced composite technologies.

GENERAL NOTE
This report is based on a presentation held at the AIAA SciTech 2022 Forum, San Diego, CA & Virtual, January 3-7, 2022.

Royal NLR
Anthony Fokkerweg 2
1059 CM Amsterdam, The Netherlands
p) +31 88 511 3113
e) info@nlr.nl i) www.nlr.nl

Dedicated to innovation in aerospace

NLR-TP-2022-004 | February 2022

Development of a Liquid Hydrogen-Based Fuel Cell System for the HYDRA-2 Drone

CUSTOMER: NLR

AUTHOR(S):

P.C. de Boer	NLR
A.J. de Wit	NLR
R.C. van Benthem	NLR

Royal NLR - Netherlands Aerospace Centre

This report is based on a presentation held at the AIAA SciTech 2022 Forum, San Diego, CA & Virtual, January 3-7, 2022.

CUSTOMER	**NLR**
CONTRACT NUMBER	**---**
OWNER	**NLR**
DIVISION NLR	**Aerospace Vehicles**
DISTRIBUTION	**Unlimited**
CLASSIFICATION OF TITLE	**UNCLASSIFIED**

APPROVED BY:		**Date**
AUTHOR	A.J. de Wit	04-02-2022
REVIEWER	B.A.T. Noordman	07-02-2022
MANAGING DEPARTMENT	A.A. ten Dam	08-02-2022

Contents

Development of a Liquid Hydrogen-Based Fuel Cell System for the HYDRA-2 Drone

P.C. de Boer[1], A.J. de Wit[2]
Royal Netherlands Aerospace Centre – NLR, Amsterdam, 1059 CM, the Netherlands

R.C. van Benthem[3]
Royal Netherlands Aerospace Centre – NLR, Marknesse, 8316 PR, the Netherlands

The aviation sector is actively pursuing a reduction to its environmental footprint. Liquid hydrogen-based propulsion is one of the key innovative technologies that is currently being explored. Before this technology can be introduced into the aviation sector, several obstacles have to be overcome such as infrastructure, propulsion system, and architecture of aircraft. To gain experience with the technology, *NLR* is currently deploying a ground-based infrastructure and developing a flight platform to assist research in this area. This paper discusses the development of the liquid hydrogen-based fuel cell system for the HYDRA-2 flight platform. In particular, this work discusses the design philosophy, material choices, relevant certification requirements for the *LH2* storage tank and conditioning system. The remaining challenges and improvements of the design are outlined as well.

I. Nomenclature

BD	=	burst disc
CO_2	=	carbon dioxide
CTE	=	coefficient of thermal expansion
D	=	outer diameter of the pressure vessel in m
GH2	=	gaseous hydrogen
H2	=	hydrogen
h_{LH2}	=	evaporation enthalpy of hydrogen in J/kg
HX	=	heat exchanger
k	=	thermal conductivity in W/(mK)
L	=	total length of the pressure vessel in m
LH2	=	liquid hydrogen
m_{H2}	=	hydrogen mass at a 95% fill rate in kg
MLI	=	multi-layered insulation
NLR	=	Royal Netherlands Aerospace Centre
P	=	averaged power in forward flight in W
P_c	=	maximum allowable vessel pressure due to stresses in the circumferential direction in Pa
P_d	=	design pressure in Pa
PED	=	Pressure Equipment Directive [8]
P_l	=	maximum allowable vessel pressure due to stresses in the longitudinal direction in Pa
P_p	=	proof pressure in Pa
PR	=	pressure regulator
P_r	=	relief pressure in Pa
PS	=	pressure switch
P_s	=	maximum allowable vessel pressure due to stresses in the spherical direction in Pa

[1] Intern, Collaborative Engineering Systems department AVCE.
[2] R&D Engineer, Collaborative Engineering Systems department AVCE.
[3] Senior Scientist, Electromagnetics, Energy Management & Qualification department ASEQ.

PV = product of maximum allowable gauge pressure and internal volume of a pressure vessel in Bar l
P_w = working pressure in Pa
$\dot{q}$ = heat flux in W/m^2
$\dot{Q}_{heater}$ = heat inflow from the heater element in W
$\dot{Q}_{insulation}$ = heat inflow through the solid insulation layer of a single wall tank in W
$\dot{Q}_{piping}$ = heat inflow through the piping in W
$\dot{Q}_{radiation}$ = heat inflow through radiation in W
$\dot{Q}_{production}$ = required heat inflow to evaporate hydrogen at the fuel cell consumption rate in W
$\dot{Q}_{support}$ = heat inflow through the structural supports in W
$\dot{Q}_{tank}$ = total passive heat inflow into the storage vessel W
$\dot{Q}_{total}$ = total heat inflow in W
r = fill rate after refueling
S = thermal shape factor for steady-state conduction
$t_{boil\text{-}down}$ = boil-down time of the storage vessel in s
t_{flight} = potential flight time in s
t_{ground} = time required for ground operations in s
T = local temperature in K
T_a = ambient temperature in K
T_c = liquid hydrogen boiling temperature in K
TS = thermistor
UAV = unmanned aerial vehicle
V = volume of the tank in m^3
VR = vent relief valve
$VTOL$ = vertical take-off and landing
α = fraction of parasitic power of the fuel cell system relative to the total power production
η = hydrogen consumption rate per unit of net output power in kg/(W s)
ρ = density liquid hydrogen in kg/m^3

II. Introduction

The aviation sector is actively pursuing a reduction to its environmental footprint. The sector releases more than 900 million tons of CO_2 per year into the atmosphere [1]. In a comprehensive study conducted by Royal Netherlands Aerospace Centre (*NLR*), a decarbonization roadmap for European Aviation is presented [2]. This roadmap predicts a 20% reduction in net CO_2 emissions from the European aviation sector in 2050 if hydrogen technology is introduced. The potential reduction of the total climate impact, including non- *CO2* sources, because of liquid hydrogen technology has recently been quantified in a study conducted by McKinsey & Company [1]. Liquid hydrogen is considered to be the most competitive form of hydrogen storage because of its high volumetric energy density compared to its gaseous phase. Hydrogen can reduce the climate impact of aircraft up to 75% and 90% for combustion and fuel cell technology respectively [1]. This exhibits the importance of the development of liquid hydrogen-based fuel cell technology.

Introducing liquid hydrogen technology into the aviation sector requires radical changes to infrastructure, the propulsion system, and possibly the complete architecture of aircraft [1]. To obtain experience with the technology and to identify areas that need improvement of existing technology, *NLR* is currently deploying a ground-based infrastructure and an *LH2*-based flight platform to support research in this area. In October 2019, the *NLR* has demonstrated a 39 minute flight of the HYDRA-1 drone using compressed hydrogen [3]. This project has been succeeded by the HYDRA-2 project, a fixed wing rotor assisted *UAV* capable of vertical take-off with a fuel cell system that is also based on hydrogen. It has been converted from a purely electric powertrain to a hybrid powertrain using compressed hydrogen and purely electric propulsion. A fairing has been added to the drone to provide additional space for hydrogen storage. The next step is to introduce *LH2* to the HYDRA-2. This paper describes the design of an *LH2* propulsion system for the HYDRA-2. The flight platform is shown in Fig. 1.

Fig. 1 The HYDRA-2 flight platform. Image – Royal NLR.

These developments are part of a long-term vision of the *NLR* to develop a lightweight hydrogen-based propulsion system.

Research has been conducted on liquid hydrogen-based fuel cell systems for *UAV*s in the past. In 2013 & 2014, flight testing results and design of a 300 W fuel cell system with a 20.46 l *LH2* tank volume have been presented by Swider-Lyons et al. & Stroman et al. [4, 5]. This project aimed to demonstrate the potential of *LH2* storage for long endurance flights. Subsequently, designs of a 498 W and a 200 W liquid hydrogen-based fuel cell system have been published [6, 7]. Both studies provide an *LH2*-based fuel cell system design but no description of flight testing of the systems has been published.

Safety assurance and compliance with the existing regulatory framework are considered to be key for conducting flight tests. *LH2*-based fuel cell systems for aeronautical applications are a new field of development and there is no single set of regulations that adequately covers all aspects of safety and quality assurance. For this work, the 'Pressure Equipment Directive' (*PED*) [8] and 'EN 13458 – part 2: Cryogenic vessels, static vacuum insulated vessels' [9] will be used as a regulatory framework for the *LH2* storage design because a ruleset for aviation vessels is not available. The scope of the *PED* excludes aviation and is limited to stationary pressure vessels, hence dynamic testing of the system is not covered by the *PED* and must be evaluated in a separate risk analysis which is not part of the work presented here. This work presents the development of a lightweight *LH2* storage tank and *LH2* conditioning system designed specifically for the HYDRA-2 platform. The main focus of this paper is the design of the *LH2* storage vessel. Relevant components that place design restrictions on the LH2 storage vessel coming from the conditioning system are discussed as well.

III. LH2 Storage Vessel Concept Study

A. Objective

The objective of this work is the development of a liquid hydrogen-based fuel cell system that can provide enough energy to the propulsion system to sustain a forward flight of at least 2 hours. The propulsion system has a battery-powered backup that is used for vertical take-off and landing. In case of complete power failure, a parachute system is present to avoid crash landings. As much existing technology as possible shall be used. Hence, although it is the desire to arrive at a lightweight composite *LH2* storage vessel, as a baseline design a metal *LH2* storage vessel will be designed and constructed.

B. Requirements

The *LH2* storage vessel design concepts that are evaluated in this section must satisfy the following main requirements:

1) Design pressure: 6 barg
2) External volume: D= Ø160 mm, L= 550 mm
3) Total tank weight including instrumentation: <4.6 kg
4) Flight time: >2 hours
5) Boil-down time: > 3.5 hours
6) Maximum heat leak: ≤ 80% of the required heating rate for cruise flight
7) Hydrogen production rate: 0-2 g/min (corresponding to 0-2 kW FC output power)
8) G-forces: x,y = ±1g , z = -1 to 4.5g

Justification for the requirements:

1) The product of vessel pressure and volume (*PV*) does not exceed 25 Bar l. This falls below the *PED* [8] category I, allowing for 'good engineering practice'. Involvement of a notified body is not required.
2) *LH2* storage and equipment shall fit inside a 550 mm x 160 mm cylinder shape (length x diameter) corresponding to the dimensions of the original (HYDRA-2A) high-pressure tank.
3) The total weight of the fuel cell system (tank and additional components) shall not exceed 8.5 kg.
4) This is considered to be the minimum for conveniently operating the drone.
5) A minimum flight time of at least 2 hours + 1.5 hour drone pre-flight preparations shall be available: $t_{boil\text{-}down} > t_{flight} + t_{ground}$. Boil-down time is defined as the time required for the complete hydrogen content to boil off without providing additional heating.
6) Excessive hydrogen venting during cruise must be avoided. A 20% design margin is applied.
7) Hydrogen demand may vary between 0-2 g/min depending on the flight modes. The power output of the fuel cell system shall be around 1500 W during cruise corresponding to a hydrogen fuel demand of 1.5 g/min.
8) Based on estimations for HYDRA-2 at cruising speed, 30° slip, and gusts.

C.Single Wall Concepts

This section explores the feasibility of *LH2* storage vessels that consist of a single metal shell with solid insulation material. Single wall storage vessels have the potential for straightforward and lightweight cryogenic storage. The single wall concepts consist of an aluminum tank shell, a solid insulation layer, two structural supports, and three stainless steel pipes. The three pipes are used as inlet, outlet, and over-pressure safety pipe, similar to the piping shown in Fig. 3. The three stainless steel pipes have a spiral shape that enhances their thermal resistance. Cryogel® is one of the best insulation materials available. An average thermal conductivity of k=0.015 W/(mK) is assumed based on product specifications. Multi-dimensional steady-state conduction for the insulation layer with varying thickness of the tank has been evaluated for various shell dimensions. The heat flow through the insulation material ($\dot{Q}_{insulation}$) is calculated through Eq. (1).

$$\dot{\boldsymbol{Q}}_{\boldsymbol{insulation}} = \mathbf{kS}(\boldsymbol{T_a} - \boldsymbol{T_c}) \tag{1}$$

Where **k** denotes the thermal conductivity of the insulation material. The *S* corresponds to the thermal shape factor, T_a the ambient temperature, and T_c the temperature of the inner vessel. Fourier's law, shown in Eq. (2) predicts a heat inflow independent of the shape of the vessel due to thermal bridging of the piping and structural supports.

$$\dot{q} = -k\frac{dT}{dx} \tag{2}$$

The variable $\dot{q}$ denotes the heat flux perpendicular to the flow direction and k corresponds to the thermal conductivity of the piping or of the structural supports. Averaged thermal conductivities of 11.34 W/(mK) and 0.30 W/(mK) have been used for the stainless-steel piping and the composite supports respectively. *T* is the local temperature and x is the coordinate in the flow direction. Starting at the outer vessel and going into the inner vessel is defined as positive x direction. The resulting heat inflow due to thermal bridging of the piping and structural supports has been added to the heat inflow through the insulation, resulting in the total passive heat flow into the storage vessel ($\dot{Q}_{tank}$). This is shown in Eq. (3).

$$\dot{Q}_{tank} = \dot{Q}_{insulation} + \dot{Q}_{support} + \dot{Q}_{piping} \tag{3}$$

In which $\dot{Q}_{support}$ corresponds to the heat inflow via the supporting structure and $\dot{Q}_{piping}$ corresponds to the heat inflow via the three pipes. Furthermore, to calculate the heat inflow into the tank, the following conditions are considered:

1) A uniform internal shell temperature distribution at 20 K (assuming a 95% fill rate at 1 bara)
2) An external surface temperature equal to the maximum ambient temperature of 303 K
3) A perfect hemispherical cylinder shape

To show how the tank dimensions of the current hemispherical cylinder shape influences the boil-down time a contour plot of the geometrical design domain is constructed. First, the boil-down time is calculated via Eq. (4).

$$\boldsymbol{t_{boil-down}} = \frac{\boldsymbol{m_{H2}h_{LH2}}}{\dot{\boldsymbol{Q}}_{\boldsymbol{tank}}} \tag{4}$$

Where h_{LH2} is the evaporation enthalpy of hydrogen and m_{H2} is the mass of the stored *H2*. Furthermore, to achieve the maximum required hydrogen production rate of 2 g/min during flight, the required heat inflow rate, $\dot{Q}_{production}$, is calculated to be *12.42W* is satisfied through Eq. (5). For a required hydrogen production rate of 1.5 g/min during cruise, 9.32 W of heat inflow is required.

$$\dot{Q}_{production} = \dot{m}_{H2} h_{LH2} \tag{5}$$

Because the passive heat leak is less than what is needed for the hydrogen production as shown in Eq. (6), a heater element is used to supplement power to produce the maximum amount of hydrogen when the fuel cell system is fully operational. The total heat inflow in the tank must always be smaller than the heat inflow corresponding to the fuel cell consumption rate to prevent excessive venting as shown in Eq. (6).

$$\dot{Q}_{tank} \leq \dot{Q}_{production} \tag{6}$$

The required supplemental heating power is calculated using Eq. (7).

$$\dot{Q}_{heater} = \dot{Q}_{production} - \dot{Q}_{tank} \tag{7}$$

$\dot{Q}_{heater}$ denotes the heat inflow from the heater element. On top of the computed heating power, a multiplication factor is recommended to achieve a faster hydrogen production rate response. In Fig. 2, the dimensional dependency of the boil-down time of the single wall tank is shown. The coloring represents the potential boil-down time based on the heat flow into the tank calculated via Eq. (4) and following the conditions stated in this paragraph.

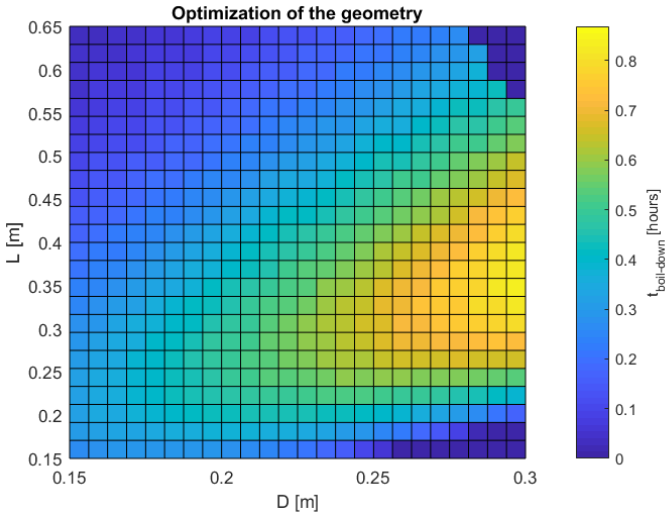

Fig. 2 Dimensional dependency of the boil-down time for a single wall tank.

The boil-down time has been computed by constructing tank geometries based on a cylindrical external volume that represents the available space under the drone characterized by length L and diameter D. The insulation thickness was increased for tank geometries at every domain point (L, D) in Fig. 2 until a heat leak arose that corresponded to 80% of the required hydrogen production rate during cruise. By doing this, the optimal ratio between insulation thickness and storage volume is found. The remaining 20% was used as a design margin for the heat leak. This modeling approach captures both the effect of change in volume due to a change in insulation thickness as well as the effect of enhanced thermal resistance due to the increased insulation thickness. Any tank geometry with excessive heat inflow is defined as having a boil-down time of zero. Near the two right side corners in Fig. 2, the heat inflow rate of these large geometries becomes too high. Because of this, requirement 6 cannot be met. The contour plot in Fig. 2 shows that increasing the diameter up to 0.3 m is beneficial for the potential boil-down time. This is because of the favorable thermal shape factor in combination with a large vessel volume. Fig. 2 shows that a single wall *LH2* tank has a maximum boil-down time of 0.8 hours and thus is not a feasible option for achieving a boil-down time of at least 3.5 hours. This also implies that the flight time requirement (requirement 4) cannot be met. In addition to this, the geometries in Fig. 2 with the most promising boil-down times do not meet requirement 2. The thermal performance of a single wall vessel is strongly dependent

on its shape and dimensions. Liquid hydrogen has a low volumetric energy density compared to conventional fuels and this also means that shape independence of the *LH2* storage vessel can be important for utilizing available space in an airframe. Structural properties are not accounted for in this section and are considered to be secondary to thermal performance. A single wall vessel has less complexity than a double wall vessel so the expected time required for completion of the design and manufacturing would be less than for a double wall tank.

It can be concluded that single wall tanks cannot meet all requirements and thus are not viable for implementation into the HYDRA-2. Double wall storage vessel concepts have subsequently been investigated.

D. Double Wall Concepts

A double wall storage vessel consists of two concentric tank shells with a vacuum in between. This minimizes heat transfer through the shells. The examined double wall concepts have two structural supports and three pipe connections, similar to the single wall concepts. The same assumptions as for the single wall concepts apply. In contrast to a single wall vessel, the shape and size are not the most important factors anymore but rather the design of the connections between the inner and outer vessel. Radiation through the vacuum layer can be significantly reduced by using multi-layered isolation (*MLI*). *MLI* is also used as a heat shield for the inner tank in case of rapid air condensation because of a loss of vacuum. Such a failure imposes an extremely high heat load on the inner tank with a large amount of hydrogen boil-off as a result. This could lead to a pressure build-up and rupture of the vessel if not designed carefully. A burst disc (*BD*) is used as a backup pressure relief mechanism to protect against this scenario. The ISO 21013-3:2016 norm prescribes design guidelines such as the maximum allowable pressure drop over the safety pipe in case of a loss of vacuum [10]. Conduction through the tank connections is a key element in the design of a double wall tank. A common approach is to increase the length of the connections in order to raise thermal resistance and minimize thermal gradients. Also, a material with a relatively low thermal conductivity should be used. The inner and outer vessel shells can be considered to have a uniform temperature. The temperature gradients in the structure arise over the connections between the inner and outer vessel. The energy balance comprises conduction through the vessel connections and the radiation between the inner and outer vessel. Convection through a good vacuum will approach zero. Any remaining convective effects through the vacuum jacket are included in the radiative heat transfer component for a certain type of *MLI* and quantified as heat loss per unit area specified by the *MLI* manufacturer which is measured under good vacuum (< 10^{-5} mbar). This heat loss per unit area is multiplied with the area of the outside surface of the inner vessel to obtain $\dot{Q}_{radiation}$. The thickness of the vacuum jacket must be sufficient to allow for placing the hydrogen piping. The double wall concept is further developed hereafter.

IV. System Design

E. System Layout

The concept study has pointed out that a double wall tank is the only type of design that can satisfy all requirements set for this project. A maximum potential flight time can be achieved for a cylindrical shape with hemispherical heads of 550 mm total length and a diameter of 160 mm. A schematic design of the storage vessel is shown in Fig. 3.

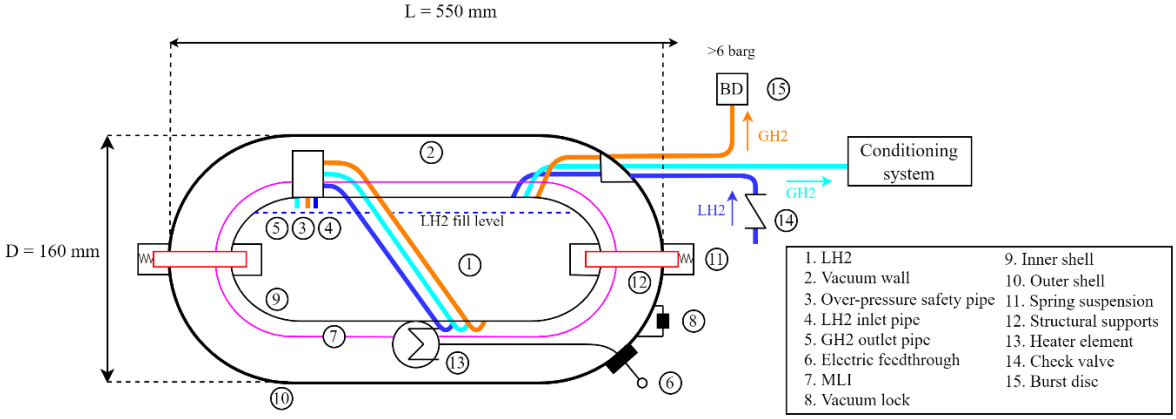

Fig. 3 System schematic of the *LH2* storage vessel.

As shown in Fig. 3, the double wall vessel can be filled up to 95%. The remaining 5% of the inner volume is reserved as margin. The spring suspension is designed to accommodate thermal contraction while keeping the

inner vessel centered with respect to the outer vessel and to be resistant to the applicable g-forces. Components of the conditioning system are described in Section M.

F. Material Selection for the Storage Vessel

This section describes how the tank shell material has been selected. Table 1 shows how the choice of material of the storage vessel influences the total system weight.

Table 1 Tank mass for different materials.

Shell material	2mm Inner shell mass in kg	2mm Outer shell mass in kg	Miscellaneous mass in kg	Total tank mass in kg
Aluminium	0.89	1.47	1.6	3.96
Stainless steel	2.64	4.35	1.6	8.59

The miscellaneous mass of 1.6 kg accounts for instrumentation and safety features. Aluminum and stainless-steel alloys are the material groups that are allowed in EN 13458-2 because of their proven cryogenic use, high strength to weight ratio, and excellent corrosion resistance [9]. Miscellaneous mass in Table 1 comprises components 3-8 & 11-15 from Fig. 3. The piping that connects both tank shells will be made out of AISI316L (stainless-steel) due to its low thermal conductivity and resistance to hydrogen embrittlement. Leak tight transition joints may be introduced at either end of the tubing to compensate for expansion difference between the materials when exposed to liquid hydrogen at 23K, large temperature gradients, and thermal cycling. Table 1 shows that aluminum alloys result in a low vessel weight and are the only material group that can satisfy requirement 3 from Section B. A 2 mm shell thickness has been used for comparison. This is because of the weldability of thin walled metal and a 1.5 mm lower limit of shells for pressure vessels according to the EN 13458-2 which is used for compliance with the *PED* [9, 11]. If there would be no lower limit on shell thickness, stainless steel tanks would achieve similar structural performance comparable to aluminum.

Different series of aluminum alloys (1XXX – 7XXX) have wide ranging material properties. Material properties are dependent on temperature and hydrogen exposure. Alloy series are evaluated on the following properties:

1) Weldability
2) Strength
3) Ductility
4) Fracture toughness
5) Sensitivity to H2 induced corrosion

Most aluminum alloy series can be welded but most of the high strength alloys (2XXX and 7XXX) are very sensitive to weld defects which reduces the as-welded material strength compared to the base metal. The 5XXX series stands out with excellent weldability [12]. The 6XXX series is weldable but can also be sensitive to weld defects. Aluminum has been selected due to its high strength to weight ratio, this means that among the readily weldable alloys, the 5XXX and 6XXX stand out. The commonly used alloys from these series will be focused on in the next subsections. Welding for low temperature applications must be done according to a welding procedure qualification which involves tensile tests at the lowest design temperature. The welding procedure qualification for AL5083 is exempted from low temperature tensile testing in the ASME Boiler and Pressure Vessel Code [11].

Aluminum alloys tend to have an increasing yield strength with decreasing temperature. So if the lowest possible yield strength is to be obtained, it should be evaluated at its maximum design temperature which is 303 K. This leads to the yield strength values of common alloys of the 5XXX and 6XXX series presented in Table 2. The AL6061-T6 outperforms the 5XXX alloys in terms of yield strength. It's important to note that the T6 temper of the AL6061 alloy increases the yield strength with respect to the O-temper. This is at the expense of elastic limit [13] and impact energy. The impact energy is measured with a Charpy test. Also, it has to be considered whether the T6 temper is compliant with potential post-weld heat treatment. AL6061-O has a very low yield strength and because of this, it will not be considered as a feasible material option.

Table 2 Material properties at different temperatures [13]. *Data deficient.

Material	Yield strength in MPa			Elastic limit in %			Impact energy in J		
	303 K	77 K	20 K	303 K	77 K	20 K	303 K	77 K	20 K
AL5083-O	152	165	*	23	33	*	*	22 (Ref. [14])	*
AL5086-O	124	131	*	27	54	38	19	16	14
AL6061-T6	275	310	372	19	24	26	12	15	16

During cool-down to cryogenic temperatures, metals can undergo a ductile to brittle transition. This transition reduces the metal's resistance to impact. This can result in a very sudden and catastrophic failure of a vessel. To

minimize this, ductility and fracture toughness at the lowest possible operating temperature should be maximized. In this case, the inner tank shell is most sensitive because it can cool down to 20 K. Material data for AL5083-O at 20 K is not available in the open literature. Hence, the material properties will be compared at the lowest available temperature of 77 K. Material data at 20 K of AL5086-O, which is a very similar alloy, is available so this information is also provided in Table 2. Ductility at these temperatures is summarized in Table 2 based on Ref. [13] unless specified otherwise. It clearly shows that the elastic limit at low temperatures of both AL5083-O and AL5086-O is significantly higher than the AL6061-T6 alloy. The fracture toughness, quantified by the impact energy, is a bit harder to evaluate due to deficient data. AL5083-O has a significantly higher impact energy at 77 K compared to AL6061-T6. At 20 K, AL5086-O has a slightly lower impact energy compared to AL6061-T6. Impact energy data of AL5083-O at 20 K is deficient.

For assessment of sensitivity to hydrogen embrittlement, two cases will be considered. First of all, hydrogen exposure at operating temperature. The second case is the exposure of weld lines to atmospheric hydrogen. According to Ref. [15], hydrogen embrittlement is most prevalent at room temperature for most materials. Because of this, hydrogen embrittlement should be evaluated at room temperature for a safe design. At cryogenic temperatures, most materials are reported to be negligibly embrittled by hydrogen. Ihara & Itoh list AL5083 as a candidate material for *LH2* tank systems [16]. According to the article, no serious hydrogen embrittlement into AL5083 has been reported although some invasion and permeation of hydrogen molecules is possible. Magnesium content is known to be an important driver for hydrogen embrittlement. The 5XXX alloy series has a high Mg content which may be cause for a small amount of embrittlement. However, the AL5086 alloy, which has a very similar composition compared to AL5083 with a maximum of 4.5% Mg vs 4.9% Mg respectively, is reported to have negligible sensitivity to hydrogen embrittlement [15]. This is similar to the AL6061-T6 alloy and all other aluminum alloys that are listed in the report. Ghorani et al. mention that local concentrations of Mg might exceed 5% due to welding and therefore embrittled zones might form [17]. While this is not reported to have caused any failures, it is recommended to evaluate carefully and potentially mitigate. Post-weld annealing can be a way to mitigate this and restore a favorable microstructure [18]. The high temperatures of the annealing process cause hydrogen to diffuse out of the metal. The effect of any potentially remaining locally embrittled zones would be assessed during mechanical testing which is part of a welding qualification procedure.

Based on the findings presented above, AL5083-O is considered to be the most suitable material for shells of the cryogenic storage vessel. An overview of the trade-off that has been made is shown in Table 3.

Table 3 Overview of the material trade-off.

Material	Weldability	Strength	Ductility	Fracture toughness	Sensitivity to H2 induced corrosion	Overall score
AL5083-O	+	-	+	+	+	+++
AL6061-T6	-	+	-	+	+	+

AL6061-T6 has a superior yield strength but an inferior ductility (at 77 K compared to AL5083-O) and weldability. Because of the relatively low pressure of the hydrogen and the lower limit of the shell thickness, yield strength is not the main driver for the material selection. The excellent weldability of AL5083-O compared to other aluminum alloys and its proven cryogenic use makes this a very pragmatic option. Also, the cryogenic ductility is favorable. There is not enough data to draw a conclusion about the fracture toughness of AL5083-O compared to AL6061-T6. No significant risks related to hydrogen induced corrosion are identified.

The usage of composite material to construct the inner and outer shell of the tank is being investigated. The challenges facing manufacturing of such a double wall cryogenic storage vessel and obtaining sufficient material data at cryogenic temperatures are currently being evaluated.

G. Structural Design of the Inner Vessel

The maximum allowable stress for AL5083-O is 78.6 MPa [11]. This value is taken at the maximum design temperature of 303 K. Design guidelines for pressure vessels are prescribed by EN 13458-2 [9]. The pressures that apply to the storage tank are listed in Table 4.

Table 4 Pressure levels in the inner vessel.

	Pressure in barg
P_w	4
P_r	5
P_d	6
P_p	9

P_w denotes the working pressure, P_r the relief pressure, P_d the design pressure, and P_p the proof pressure. The structural design pressure for the design has been set at 6 barg. The proof pressure has been set at 1.5 times the design pressure. The inner vessel internal volume is 3.9 l which leads to a product of pressure and volume (PV) of 23.4 Bar l. This classifies below category I according to the Pressure Equipment Directive [8] allowing for 'good engineering practice'. Involvement of a notifying body is not required for this category. Maximum allowable internal pressure can be analyzed based on calculating the stresses in the longitudinal, circumferential and spherical direction. This is done by assuming zero corrosion allowance. Dynamic loading is not considered. The hoop stress calculation applies to the shells of the inner tank. Any stress concentrations and shapes that diverge from a perfect hemispherical cylinder are not considered here. This leads to the allowable pressures in Table 5 that show that a design pressure of 6 barg is 4.4 times less than the allowable pressure.

Table 5 Structural properties of the inner vessel shell.

	Allowable pressure in barg
P_l	55.3
P_c	26.6
P_s	54.0

P_l, P_c, and P_s denote the allowable pressure in the longitudinal direction, circumferential, and spherical direction, respectively. The inner vessel contracts 2.1 mm in the longitudinal direction during cool down. Additionally, the diameter of the inner vessel contracts 0.45 mm. The design of the piping between the two shells is designed to be able to undergo these displacements.

H. Structural Design of the Outer Vessel

The outer vessel shell is subjected to a maximum external pressure of 1.013 barg under full vacuum. Evaluation of the structural integrity should be conducted with a different method than for a vessel subjected to internal pressure. The pressure calculations for the external pressure on the outer shell are based on Ref. [11]. An allowable external pressure of 3.1 bar results from this evaluation. Thus, the 2 mm thick AL5083-O shell can withstand 3.1 times the maximum applied external pressure.

I. Structural Supports

The structural supports are used to position the inner vessel shell with respect to the outer vessel while accommodating thermal contraction and the expected G-forces in x,y, and z direction. Fig. 4 shows the cross-section of the supports.

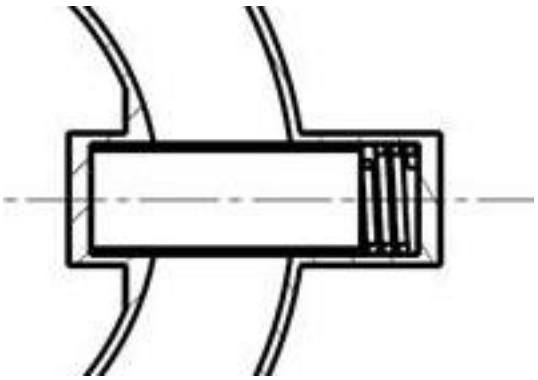

Fig. 4 Cross-section of the structural supports.

A glass fiber composite, G-10 CR, is used for construction of the rods based on an excellent ratio between the thermal conductivity and strength. The G-10 CR composite is specifically intended for cryogenic use. The rods are designed to withstand the shear and bending loads induced by g-forces in the z and y direction. G-forces in the x direction are absorbed by compression springs that can undergo limited displacement to prevent excessive deformation of the piping. The maximum displacement of the inner vessel causes exclusively elastic deformation of the hydrogen piping. The springs also keep the inner vessel centered while contracting during cool-down of the vessel.

J. Thermal Analysis

A discretized 1D model has been created to evaluate thermal conduction through the piping and supports. Material dependent properties are based on data from the National Institute of Standards and Technology (NIST). It is assumed that there is no radial heat flow in the pipes and supports. Both the inner and outer tank shell are considered to have a uniform temperature at 20 K and 303 K, respectively. Heat flow through the vacuum layer is accounted for by using product specifications from the Coolcat® LOX *MLI* which accounts for both radiation and conduction under good vacuum (< 10^{-5} mbar). Fourier's law, recall Eq. (2), has been used to evaluate thermal conduction in the discretized 1D domain. Material properties are evaluated at their respective temperatures. The supports are assumed to have a thermal resistance based on their length through the vacuum layer. The support material is a G10-CR glass fiber composite. Thermal edge effects are not included. Also, the piping geometry has been simplified to a straight AISI316L pipe of 0.56 m in length. The resulting heat flow components are shown in Table 6.

Table 6 Heat flow components.

Component	Heat flow in W
$\dot{Q}_{piping}$	0.24
$\dot{Q}_{radiation}$	0.56
$\dot{Q}_{support}$	0.62
$\dot{Q}_{total}$	1.42

The presented heat flow components enable resolving the heat balance shown in Eq. (8) for determining the total heat inflow into the LH2 storage vessel ($\dot{Q}_{total}$) including heat flow from the heater element.

$$\dot{Q}_{total} = \dot{Q}_{support} + \dot{Q}_{piping} + \dot{Q}_{radiation} + \dot{Q}_{heater} \tag{8}$$

The boil-down time of the double wall concepts can be computed with Eq. (3) and Eq. (4) based on the computed passive heat inflow ($\dot{Q}_{tank}$) of 1.42 *W*. The computed boil-down time is 15.7 hours which is well above the 3.5 hours requirement. To achieve the required maximum hydrogen production rate of 2 g/min, 11 W needs to be additionally supplied with a polyimide heater element which is placed inside the vacuum jacket on the outer surface of the inner vessel.

K. Anticipated Flight Duration

The requirement for a flight duration of >2 hours largely depends on the drone performance such as fuel consumption, tank fill rate and the preparation time before take-off. The amount of hydrogen stored and the boil-down time is fully determined by the design of the tank. The flight duration can be computed based on the total amount of hydrogen stored in the tank and the averaged fuel consumption of the drone. The potential flight time (t_{flight}) can be estimated with Eq. (9) by assuming a constant power consumption during cruise.

$$t_{flight} = \frac{\rho V\, r\, (1-\alpha)(1-t_{ground}/t_{boil-down})}{P\, \eta} \tag{9}$$

The density is denoted with ρ, the storage volume with V, and the fill rate with r. The α represents the fraction of parasitic power of the fuel cell system relative to the total power production. The average power in forward flight is denoted with P. The hydrogen consumption rate per unit of net output power is represented by η. Evaluating the equation results in a potential flight time of 2.2 hours while assuming a 95% fill rate, a parasitic load fraction of 0.23, and a 0.8 g/(min kW) hydrogen consumption rate per unit power.

L. Transition Joints

The inner and outer shell of the LH2 storage vessel consist of an aluminum skin. The connection between the inner and outer skin via piping introduces a conductive heat leak through the piping. Hence, to avoid heat loss through the piping a material is selected that acts as a thermal barrier. In the present case, stainless steel piping is selected because the heat conductance is much less than that of aluminum. To join aluminum and stainless steel several possibilities exist. For example, friction stir welded joints, see Fig. 5.

Fig. 5 Example of bi-metal welded joints that could be used to join stainless steel tubing to aluminum vessel. Image - Royal NLR.

Joining two materials that have different coefficients of thermal expansion (*CTE*) such as aluminum and stainless steel causes one material to shrink/expand more than the other material resulting in high stresses in the joining area. The temperature decrease considered in the present work (approximately 280 K) is expected to cause joint failure for bi-metal joints. Hence, welding may prove to be difficult. With careful selection of the temperature profile while joining and geometry design of the joint some of the difficulties, may be overcome but this has to be studied further. A third material to bridge the *CTE* mismatch may be required.

Another possibility is to use a crimp fitting. In this case, aluminum is heated before it is joined with the stainless-steel. When the aluminum and stainless-steel are cooled down to ambient and cryogenic temperatures, the *CTE* mismatch causes the aluminum to shrink such that the stainless steel is locked within the aluminum. The fit causes stresses at the interface, the values of which are dependent on the diametral interference, that can be less critical than those observed in a weld with *CTE* mismatch. Leakage of the joint should be investigated which is critical for maintaining a vacuum in the vessel wall.

To summarize, detailed analysis and design optimization of the connection between the piping and the inner and outer skin is necessary to create a leak proof joint that can sustain the temperature cycles that are foreseen.

M. Conditioning System

This section describes the design philosophy of the hydrogen conditioning system. The function of the conditioning system is to supply the two fuel cells with a hydrogen stream at the desired pressure and temperature. All components described here have been selected based on weight and compactness. A schematic overview of the conditioning system is shown in Fig 6.

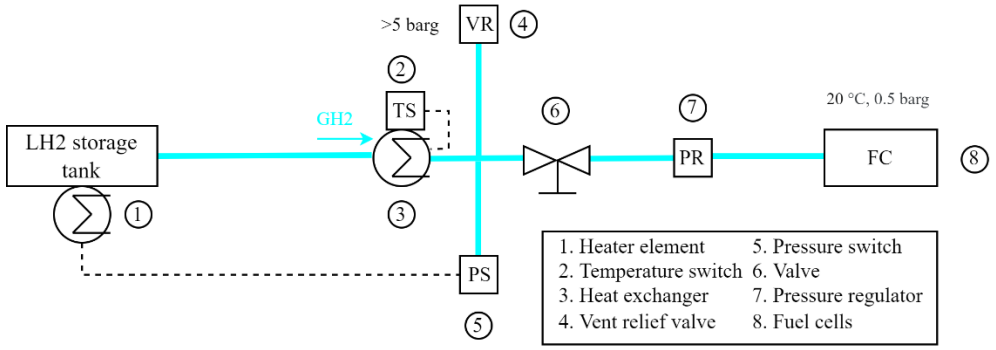

Fig. 6 Schematic design of the conditioning system.

The HYDRA-2 drone is powered by two IE-Soar™ 800W fuel cells. A 1500W power output is required for cruise flight so both fuel cells operate at 94% of their maximum continuous power. The two fuel cells combined require a hydrogen mass flow of 1.5 g/min at 0.5 barg ± 0.25 barg with a temperature of more than zero degrees Celsius. The standard hydrogen regulator cannot be used in combination with the *LH2* vessel design presented in this paper because the working pressure is too low to establish sufficient hydrogen flow to the fuel cell. A forward pressure regulator (*PR*) is used instead. This is an electronically controlled pressure regulator that doesn't require a large pressure differential for establishing the required hydrogen flow rate. A custom heat exchanger (*HX*) design is made to warm up the hydrogen. Its temperature is electrically controlled with a thermistor (*TS*). The custom design *HX* is extremely compact and has a mass of only 130 g. A Generant 1/8" vent relief valve (*VR)* with a set pressure of 4 barg are used for hydrogen venting. The operating temperature range is insufficient for cryogenic hydrogen use. This is why the *VR* is placed downstream of the heat exchanger (*HX*). This ensures that the highest possible flow rates can be safely accommodated and that over-pressurization can never occur. The outlet of both the *VR* and the *BD* should be connected to a vent host that leads to a safe discharge location. A pressure switch (*PS*) is connected to the inner vessel heating element. If the pressure falls below the set operating pressure, the heater will be turned on until the target operating pressure is reached again. A Swagelok® VCR coupling will be

used to interface to the *LH2* supply. Weight measurements could be used to determine the fill level of the vessel. All components add up to a conditioning system weight of 2.96 kg.

V. Preliminary Conclusions and Outlook

The preliminary result of the current work presented is that a double wall aluminum pressure vessel in combination with a compact and lightweight conditioning system is the only feasible design option for liquid hydrogen storage onboard the HYDRA-2 drone that can satisfy all the requirements. Furthermore, particular care has to be taken for the aluminum welding process and regulatory requirements. Also, the transition joints and tank supports require careful design. Manufacturing and construction of the liquid hydrogen fuel cell system are currently in progress and a demonstration flight is expected in the second half of 2022. Further development of the cryogenic tank system involves the application of composite material for the cryogenic storage vessel that will be embedded in the HYDRA-3 platform that incorporates design improvements with respect to the current HYDRA-2 platform.

References

[1] "Hydrogen-powered Aviation: a Fact-based Study of Hydrogen Technology, Economics, and Climate Impact by 2050," McKinsey & Company, 2020.
[2] Sman , E.S. van der, Peerlings, B., Kos, J., Lieshout, R., Boonekamp, T., "Destination 2050," NLR-CR-2020-510, 2020.
[3] Benthem, R. C. van, Boer, A. I. de, Vorst, J. van der, Doorn, W.B. van, "Hydrogen Drone Research Aircraft," *Aerospace Europe Conference*, Bordeaux, France, February 2020.
[4] Swider-Lyons, K., Stroman, R., Rodgers, J., Edwards, D., Mackrell, J., "Liquid Hydrogen Fuel System for Small Unmanned Air Vehicles," AIAA Paper 2013-0467, January 2013.
[5] Stroman, R.O., Schuette, M.W., Swider-Lyons, K., Rodgers, J.A., Edwards, D.J., "Liquid Hydrogen Fuel System Design and Demonstration in a Small Long Endurance Air Vehicle," *International Journal of Hydrogen Energy*, Vol. 39, No. 21, July 2014, pp. 11279-11290.
doi: 10.1016/j.ijhydene.2014.05.065
[6] Adam, P., Leachman, J., "Design of a Reconfigurable Liquid Hydrogen Fuel Tank for Use in the Genii Unmanned Aerial Vehicle," *Proceedings of the Cryogenic Engineering Conference – CEC: Advances in Cryogenic Engineering*, 1573, Anchorage, 1299-1304, 2014.
doi: 10.1063/1.4860856
[7] Garceau, N.M., Kim, S. Y., Lim, C. M., Cho, M. J., Kim, K. Y., Baik, J. H., "Performance Test of a 6 L Liquid Hydrogen Fuel Tank for Unmanned Aerial Vehicles," *IOP Conference Series: Materials Science and Engineering*, Vol. 101, IOP, Tucson, 2015, pp. 12130-12137.
doi: 10.1088/1757-899X/101/1/012130
[8] "Directive 2014/68/EU of the European Parliament and of the Council," *Official Journal of the European Union*, 2014.
[9] "NEN-EN 13458 – part 2: Cryogenic vessels, static vacuum insulated vessels," 2002.
[10] "NEN-EN-ISO-21013-3 Cryogenic vessels – Pressure-relief Accessories for Cryogenic Service – Part 3: Sizing and Capacity Determination," 2016.
[11] "ASME Boiler and Pressure Vessel Code Division 1 Section VIII Rules for Construction of Pressure Vessels," 2019.
[12] Nakata, K., Gon Kim, Y., Ushio, M., Hashimoto, T., Jyogan, S., "Weldability of High Strength Aluminum Alloys by Friction Stir Welding," *ISIJ International*, Vol. 40 (Supplement), 2000, pp. S15-S19.
doi: 10.2355/isijinternational.40.Suppl_S15
[13] McClintock, R.M., Gibbons, H.P., "Mechanical Properties of Structural Materials at Low Temperatures ," National Bureau of Standards, Monograph 13, June 1960.
[14] Huang, C., Wu, Z., Huang, R., Wang, W., Li, L., "Mechanical Properties of AA5083 in Different Tempers at Low Temperatures," *IOP Conference Series: Materials Science and Engineering*, Vol. 279, IOP, Madison, 2017, pp. 12002.
[15] Lee, J.A., "Hydrogen Embrittlement," NASA/TM-2016-218602, 2016.
[16] Ihara, T., Itoh, G., "Behaviour of Hydrogen in Al-Mg Alloys Investigated by Means of Hydrogen Microprint Technique," *Journal of Japan Institute of Light Materials*, Vol 53, No. 12, 2003, pp. 575-581.
[17] Ghorani, A., Itoh, G., Ohbuchi, T., Kiuchi, T., "Humid Gas Stress Corrosion Cracking in MIG-Welded 5083 Aluminum Alloy Plate," *Journal of Japan Institute of Light Materials*, Vol. 61, No. 2, 2020, pp.330-338.
doi: 10.2320/matertrans.L-M2019865
[18] Brown, W., "Safety Standards for Hydrogen and Hydrogen Systems," NASA/TM-112540, 1997.

Dedicated to innovation in aerospace

Royal NLR - Netherlands Aerospace Centre

NLR operates as an objective and independent research centre, working with its partners towards a better world tomorrow. As part of that, NLR offers innovative solutions and technical expertise, creating a strong competitive position for the commercial sector.

NLR has been a centre of expertise for over a century now, with a deep-seated desire to keep innovating. It is an organisation that works to achieve sustainable, safe, efficient and effective aerospace operations.
The combination of in-depth insights into customers' needs, multidisciplinary expertise and state-of-the-art research facilities makes rapid innovation possible. Both domestically and abroad, NLR plays a pivotal role between science, the commercial sector and governmental authorities, bridging the gap between fundamental research and practical applications. Additionally, NLR is one of the large technological institutes (GTIs) that have been collaborating over a decade in the Netherlands on applied research united in the TO2 federation.

From its main offices in Amsterdam and Marknesse plus two satellite offices, NLR helps to create a safe and sustainable society. It works with partners on numerous programmes in both civil aviation and defence, including work on complex composite structures for commercial aircraft and on goal-oriented use of the F-35 fighter. Additionally, NLR helps to achieve both Dutch and European goals and climate objectives in line with the Luchtvaartnota (Aviation Policy Document), the European Green Deal and Flightpath 2050, and by participating in programs such as Clean Sky and SESAR.

For more information visit: **www.nlr.org**

Postal address
PO Box 90502
1006 BM Amsterdam, The Netherlands
e) info@nlr.nl **i)** www.nlr.org

Royal NLR
Anthony Fokkerweg 2
1059 CM Amsterdam, The Netherlands
p) +31 88 511 3113

Voorsterweg 31
8316 PR Marknesse, The Netherlands
p) +31 88 511 4444